Numerical Studies of Three-Dimensional Breakdown in Trailing Vortex Wakes

J. E. Hackett* and P. F. Evans†
Lockheed-Georgia Company, Marietta, Ga.

Finite-element three-dimensional relaxation methods are used to calculate the development of vortex wakes behind aircraft for a significant downstream distance. The inclusion of a self-induction term in the solution, dependent upon local curvature and vortex core radius, permits calculation of finite lifetimes for systems for which infinite life would be predicted two-dimensionally. Single-pair, twin-pair, and multiple-pair studies are described. It is found, in single-pair studies, that there is a lower limit to the wavelengths at which the "Crow"-type of instability can occur. Below this limit, self-induction effects cause the plane of the disturbance waves to rotate counter to the vortex direction. Self-induction in two-dimensionally generated twin spiral waves causes an increase in axial length, which becomes more marked with decreasing initial wavelength and the time taken for vortex convergence toward the center plane is correspondingly increased. In many cases designed to produce early vortex convergence at the center plane, it is found that the surviving vortex is sufficiently strong for significant hazard to remain. Such cases, which have low flap span, are also characterized by long-wavelength spirals, for which the potential for self-induced wake dispersion is small. There may therefore be a maloptimum flap-span ratio, in the mid-semispan range, for which time-to-converge maximizes. Limited studies of Boeing 747 configurations show correct qualiative response to removal of the outer flap and to gear deployment, as compared with wind-tunnel and flight-test experience.

I. Introduction

DURING the past several years, strenuous efforts have been made to devise means for breaking up prematurely and permanently the trailing vortices behind large transport aircraft so as to reduce or eliminate their hazard to following aircraft. Many of the attempts aimed at modifying individual vortices have met with indifferent success or have been impractical or too costly to apply.

Vortex looping and multiple-vortex convergence at the center plane are among the more reliable "natural" modes of vortex decay. Single-pair vortex looping was analyzed first by Crow,[1] using linear methods. Shortly thereafter, his results were extended numerically by Hackett and Theisen,[2] who calculated the progression from Crow's sinuous shapes toward the familiar "looped" form sometimes observed in flight[3] or in water-tank experiments.[2,4] The calculations used finite-element, time-dependent techniques applied to single vortex pairs.

The objective of the present work is to deepen the previous single-pair studies and extend them to multiple-pair configurations, including both wakes typical of current jumbo jets and experimental cases such as "sawtooth" loading suggested by Rossow[5] for promoting early wake disruption. Appropriate Fortran algorithms have been written and documented[6] that achieve these objectives.

The decay of a complex multivortex wake involves successive reductions in the number of vortices, either via convergence at the center plane or by merging of two vortices into one.[7] Figure 1 shows how the length of the wake may be partitioned on this basis. The terms "near," "middle," or "far wake" relate only to the number of vortices present and have no specific counterparts in miles.

Starting at the downstream end, we see that the "far" wake contains just one vortex pair. Since this has the potential for very long life under calm conditions, it is important to design the initial wake configuration in such a way that this remaining pair is a weak one. It will be shown that, with suitable starting conditions, early convergence of stronger pairs is possible.

The "middle" wake involves a twin pair. This may be treated either using parametric results or on a specific basis depending upon whether the geometry is near-spiral or has suffered noticeable distortion in the near wake. It will be shown that if middle wake parameters are properly chosen, the far wake need not be hazardous.

The "near" wake also determines the number, the strengths, and the positions of vortices that persist. Although it is possible to force certain vortices to converge to the center plane and dissipate there, it is also important to ensure that any remaining vortices will not be long-lived. For example, it may be preferable to leave a third vortex in a wake, which will disrupt an otherwise stable twin pair, rather than have it converge early at the center plane.

There is an important distinction between the instability of a spiral wave and that of a plane wave of the "Crow" type. Figure 2 illustrates this distinction from the viewpoint of an observer fixed in space. When a vortex trail with plane waves reaches a sufficient age, this observer sees "necking" start to occur, followed by a "click" when looping occurs. Thereafter, the looping point remains fixed in space. In contrast, a spiral wave is fed continuously toward the center plane. Prior to the critical time, the fixed-observer sees a convergence event moving toward him in the direction of aircraft motion. The "time-to-converge" corresponds to its passage directly in front of him. In contrast to the previous case, the event is steady as seen from an aircraft frame of reference. These considerations in no way preclude space-fixed events due to atmospheric disturbance or other modes of instability. However, to underline the distinction, the destruction of spiral waves by meeting at the center plane will be termed "convergence" in the present study and "looping" will be reserved for the space-fixed event.

In any theoretical approach like the present one, it is very desirable to make comparisons with experimental results. Documented flow investigations in the near-field are quite

Presented as Paper 76-416 at the AIAA 9th Fluid and Plasma Dynamics Conference, San Diego, Calif., July 14-16, 1976; submitted Aug. 30, 1976; revision received July 27, 1977.
Index categories: Aerodynamics; Computational Methods.
*Scientist, Lockheed-Georgia Company. Member AIAA.
†Aerodynamics Engineer, Senior, Lockheed-Georgia Company.

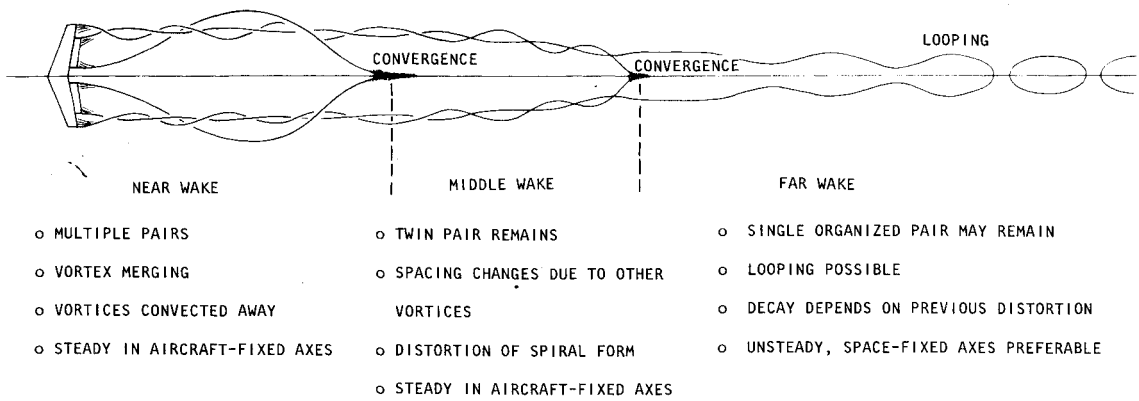

Fig. 1 Wake regions for a multiple-vortex pair.

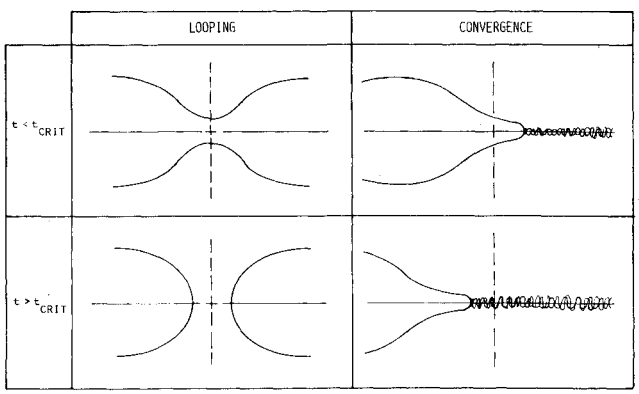

Fig. 2 The distinction between vortex "looping" and "convergence."

numerous, and there is wealth of longer-time measurements at discrete downstream planes. However, it has proved impossible to find quantitative experiments that give adequate details of vortex looping flow in three dimensions. Experiments with towed models are the most suitable for this, and, although looping has been noted with a small model size relative to the test region cross section,[2] the majority of scale models tested have been larger in size and looping has not occurred. In some cases, wall constraints may have inhibited looping; in others the vortices have encountered a horizontal surface before looping had time to occur. Even with the looping flow properly generated, good measurements are difficult.

Section II will outline the theoretical approach, velocity calculation methods, self-induction effects, and stepping procedures. Section III is devoted to single vortex pair events and further examines the vortex looping phenomenon. In Sec. IV twin- and multiple-pair events are reviewed with particular emphasis on desirable flap configurations and upon the strengths of surviving vortices. Conclusions are given in Sec. V.

II. The Calculation Method

A. General Approach

Three-dimensional relaxation calculations are carried out starting from an approximate result, which is usually determined from an unsteady, two-dimensional treatment. Element velocities are calculated via far-field (straight, axial line vortices), intermediate-field ("point" vortex elements), near-field (inclined line vortices), and self-induction equations. These are used in conjunction with a predictor-corrector stepping method. Section IIB gives further details.

It is appropriate to analyze vortex looping in a space-fixed frame of reference, as was done in Ref. 2. Monitoring such a calculation is difficult because the motion is both three-dimensional and unsteady. To relieve the problem, a computer graphics scope was employed to display the results and proved particularly useful during program development.

The time taken for a vortex pair to attain the looped state is of interest in relation to the vortex hazard problem, but there are difficulties in defining both the start and the finish of the process. All that can be done at the start is to define an initial amplitude and wavelength and assign to this state the value "TIME = 0." Despite the fact that the mechanism of the looping event itself is not well understood, it is found that the onset of rapid downward convection at the point of close approach provides a sharp and quite adequate definition of the onset of instability. The specific definition used here is that looping occurs when the greatest downward velocity exceeds ten times the original mean downdrift velocity.

The simplest multiple-vortex wake is the twin-pair spiral. Since this rotates in relation to a fixed observer, yet appears steady to an observer moving at aircraft speed, it is clearly advantageous to make calculations in aircraft-fixed axes. Unfortunately, this brings with it the need to consider simultaneously a very long length of wake. In Sec. IIC, a hybrid "sliding frame" method is described that solves the aircraft-fixed problem quite economically using techniques that closely resemble a space-fixed calculation.

B. Relaxation Calculations

Near Field

The self-induced velocity is determined in a manner similar to that of Leonard.[8] The self-induced velocity (V_s) is in a direction normal to the local plane of curvature and is given by the relation

$$V_s = \frac{\Gamma}{4\pi R_c}\left[\log_e\left\{\frac{8R_c}{\delta}\right\} - 0.558 - \frac{1}{2}\log_e\left\{\cot\frac{\theta_1}{4}\cot\frac{\theta_2}{4}\right\}\right] \quad (1a)$$

where

$$\frac{d\delta^2}{dt} = 4\nu - \frac{\delta^2}{l}\frac{dl}{dt} \quad (1b)$$

The terms in Eq. (1b) yield, respectively, the viscous growth and vortex stretching effects. Since molecular viscosity has been used in the present calculation, viscous growth is very small. Equation (1b) is evaluated in finite-difference form.

The velocity due to other vortices in the near-field is calculated using a conventional line-vortex equation, modified for core effects where appropriate.

Intermediate Field

The velocity componets at a point x,y,z are given in Ref. 9 as

$$u = \frac{\Gamma}{4\pi}\int_A^B \left\{\frac{dy'}{ds'}\frac{z-z'}{r} - \frac{dz'}{ds'}\frac{y-y'}{r}\right\}\frac{ds'}{r^2} \quad (2a)$$

$$v = \frac{\Gamma}{4\pi}\int_A^B \left\{\frac{dz'}{ds'}\frac{x-x'}{r} - \frac{dx'}{ds'}\frac{z-z'}{r}\right\}\frac{ds'}{r^2} \quad (2b)$$

$$w = \frac{\Gamma}{4\pi}\int_A^B \left\{\frac{dx'}{ds'}\frac{y-y'}{r} - \frac{dy'}{ds'}\frac{x-x'}{r}\right\}\frac{ds'}{r^2} \quad (2c)$$

where AB is an arbitrary vortex line, s' is the distance along it, and $r^2 = (x-x')^2 + (y-y')^2 + (z-z')^2$. Prime denotes a position on AB.

Converting Eqs. (2) to finite element form, we obtain

$$u_N = \sum_{L=1}^{L_{\text{total}}} \left[\frac{(\Gamma\Delta y)}{4\pi r_{NL}^3}(z_N - z_L) - \frac{(\Gamma\Delta z)}{4\pi r_{NL}^3}(y_N - y_L)\right] \quad (3a)$$

$$u_N = \sum_{L=1}^{L_{\text{total}}} \left[\frac{(\Gamma\Delta z)}{4\pi r_{NL}^3}(x_N - x_L) - \frac{(\Gamma\Delta x)}{4\pi r_{NL}^3}(z_N - z_L)\right] (N \neq L) \quad (3b)$$

$$w_N = \sum_{L=1}^{L_{\text{total}}} \left[\frac{(\Gamma\Delta x)}{4\pi r_{NL}^3}(y_N - y_L) - \frac{(\Gamma\Delta y)}{4\pi r_{NL}^3}(x_N - x_L)\right] \quad (3c)$$

where Δx, Δy, and Δz are the components of a straight, finite element that represents a segment of the vortex AB. When $N=L$, Eq. (1a) is used. In implementing Eqs. (3) for $N \neq L$, a "short element" concept is applied, in which the products, $\Gamma\Delta x_L$, $\Gamma\Delta y_L$, and $\Gamma\Delta z_L$ are defined as the short element strength components. Dummy points are situated midway between the perturbed points along each vortex line and used to determine vortex stretching. Thus, the intermediate field can be considered, without changing the total number of points, by suitable modifications to $\Gamma\Delta x_L$, $\Gamma\Delta y_L$, and $\Gamma\Delta z_L$.

When studying the periodic cases, it is convenient to use imaging techniques such that only one side of the aircraft wake and only one half-wave (one full wave for spiral perturbations) are actually perturbed and the periodic part of the wake vortex system is represented by various reflections. In the case of multivortex aircraft-fixed analysis, there is no periodic geometry, but half-plane symmetry still applies.

Far Field

Beyond one or two complete wavelengths, each side of a perturbed point, the vortex system may be extended by horizontal straight-line elements. These are added at both ends of periodic geometries (space-fixed) and at the downstream end of aircraft-fixed geometries.

Stepping Method

A one-step, second-order, predictor-corrector computation is used in which the desired element x-displacement, for example, is defined as the midpoint of the resultant of two Euler displacement vectors, $u(t)dt$ and $u(t+dt)dt$. $u(t)$ is the induced velocity field based on the positions of the vortex element system at the time t and $u(t+dt)$ is the induced velocity based on the positions of the system at time $(t+dt)$. The general relation for displacement using predictor-corrector stepping is:

$$x'(t+dt) = \tfrac{1}{2}[x(t) + x(t+dt) + u(t+dt)\cdot dt] \quad (4)$$

where $x(t+dt) = x(t) + u(t)dt$, $x(t)$ is the value at t, and $x'(t+dt)$ is the predictor-corrector value at $(t+dt)$. The other two components are treated similarly.

In two-dimensional calculations, the accuracy of the time-integration may be checked fairly readily by determining the vortex center of gravity, moments, and the Kirkoff-Routh path function (see Ref. 5). Such checks are generally not available for three-dimensional motions. In principle, checks should be made that conservation laws are obeyed, but the necessary integrations are more difficult and more numerically hazardous than the original calculation. The only check found feasible so far is to employ a reversed-marching technique to find the degree of accuracy to which the system returns to its original state. At the end of a series of time steps, the sign of the time increment is reversed, and the program marches back to the initial time. The mean deviation of each element from its initial position is then calculated and arithmetic and geometric mean errors are determined.

C. The Sliding-Frame Aircraft-Fixed Calculation Method

Figure 3 shows the progress of an aircraft-fixed three-dimensional vortex wake relaxation at successive times during the calculation. Disturbances originating near the trailing edge propagate away at approximately mainstream speed leaving a stable vortex system whose transverse velocities are near the limit of computer resolution. The vertical arrows depict the downstream end of the converged region. Let us define the propagation speed of this convergence as β times aircraft speed. We may choose a time, in the aircraft-fixed calculation, at which direct wing influence is no longer felt at the position of the disturbance front: "TIME = 20" is suitable (Fig. 3). A calculation frame, stretching, say from Station 16 to Station 28, is now drawn around the disturbance front. If this frame is slid along the wake at β times mainstream speed, the disturbance front remains centered and converged wake is always contained in the left half of the frame. If suitable precautions are taken with conditions at the ends of the frame, particularly upstream, this provides an attractive and economical basis for a wake solution. In fact, if $\beta = 1$, the algorithm is the same as for a space-fixed calculation.

The above method shows considerable promise. However, most of the results in the present paper were calculated using the earlier methods.

III. Single-Pair Looping

A. Significant Parameters

For a given vortex spacing b, the time to loop t_l is a function of the vortex strength Γ, the amplitudes a_x, a_y, phase β,

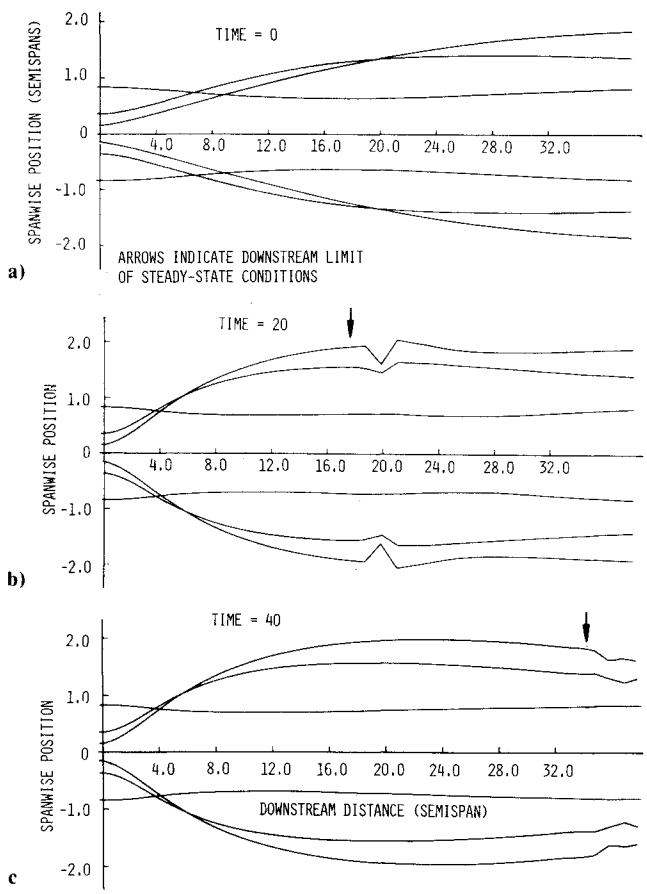

Fig. 3 Three-dimensional relaxation of multiple pairs to a steady state.

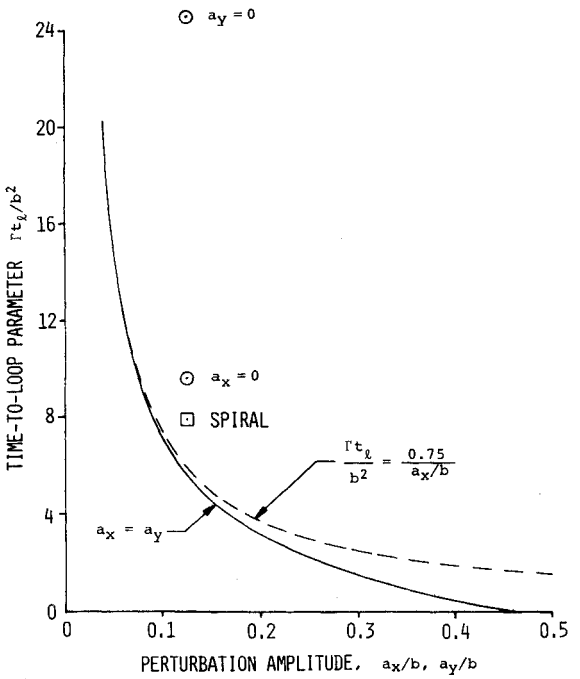

Fig. 4 Dependence of time-to-loop upon initial perturbation amplitude, $\lambda = 5.0$, $\delta/b = 0.098$.

and wavelength λb of the initial perturbation and the vortex core radius δ. The relationships take the nondimensional form

$$\frac{\Gamma t_l}{b^2} = f\left\{\frac{a_x}{b}, \frac{a_y}{b}, \beta, \frac{\delta}{b}\right\} \tag{5}$$

If a_x and a_y are in phase, the classical 45-deg inclined plane wave is obtained. With a given wavelength and core radius, time-to-loop is inversely proportional to initial amplitude (Fig. 4) and becomes zero as the wave trough approaches the center plane. If only vertical perturbations are applied ($a_x = 0$), t_l increases approximately 20%. In contrast, a wave in a horizontal plane is relatively stable and takes several times as long to loop.

Shifting the phase β between a_x and a_y to $\pi/2$ yields a spiral wave. This increases time-to-loop by approximately 40%, compared with the classical, 45-deg inclination case.

As might be expected, an increase in core radius reduces self-induction and slows down progression towards looping. For a 45-deg wave with $a_x = a_y = 0.1b$, $\lambda = 5$, and $\delta = 0.16$, doubling the vortex core radius adds about a third to t_l. This trend continues with increasing core radius until the cores touch. It was also noted that the omission of the self-induction term, as in earlier work, produced wave shapes very similar to those for a specific value of vortex radius. The effect is clearly dependent upon the number of elements used per wave and must also be present when a "cutoff" radius is employed, as in Ref. 1.

A number of investigators have suggested devices for diffusing individual vortices to reduce their hazard to following aircraft. The present result suggests that such diffusion may actually increase the time to ultimate decay, by delaying looping. It is therefore important to be certain that such attempts to accelerate diffusion have a sufficient effect.

B. Effect of Perturbation Wavelength

Figure 5 shows time-to-loop as a function of wavelength for several different values of initial, 45-deg perturbation amplitude. The right-hand part of each curve shows the expected increase in t_l, with wavelength, as reported previously.[2] However, an unexpected upturn in the curves occurred at short wavelengths giving a minimum wavelength below which

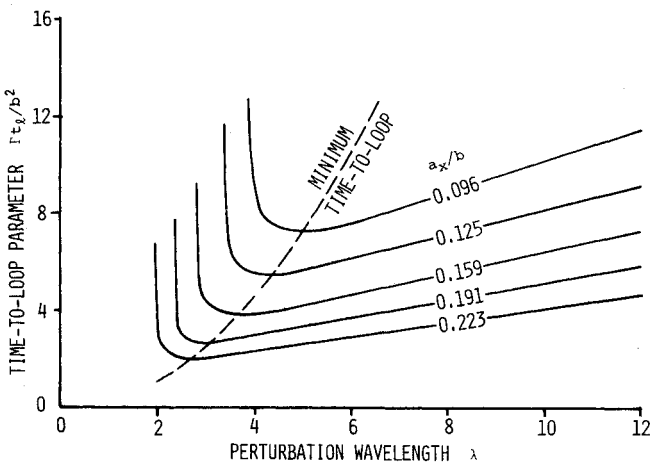

Fig. 5 Dependence of time-to-loop upon perturbation wavelength and amplitude, $a_x/b = a_y/b$, $\delta/b = 0.098$.

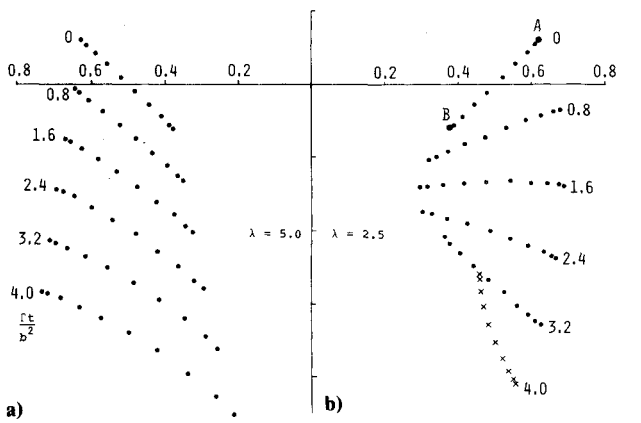

Fig. 6 End views of single-vortex pair distortion: a) distortion toward looping, $\lambda = 5.0$; b) distortion at sublooping wavelength, $\lambda = 2.5$. Note – distances are normalized on mean vortex spacing.

looping did not occur. A minimum time-to-loop is also implied.

To better understand the mechanisms, we shall examine the time history in two distinct calculations for long and short wavelengths. The left half of Fig. 6 shows end views at successive times of a 45-deg, $\lambda = 5$ wave as it progresses toward looping. As time progresses, the vortex elements drift downward, largely maintaining their 45-deg inclination. At the two longest times shown, the lower points are moving downward and inward at an increasing rate – a nascent looping stage has been reached.

The right half of Fig. 5 has essentially the same initial conditions, but a shorter wavelength. Initially, the innermost vortices move inward as before but at a faster rate, as would be expected from previous experience concerning wavelength effects. However, the 45-deg inclination is not retained as before. A clockwise rotation, opposing the direction of the vortex, develops. In consequence, the distance-of-closest approach starts to increase markedly and looping is forestalled.

The mechanism for this motion is illustrated in Fig. 7 by means of velocity vectors at the crest and the trough of one wave. The mean downward vector has been excluded in the interests of clarity. The resultant velocities, V_{res}, at A and B comprise strain components V_{LH} which are vertical, and self-induced components V_{ring} normal to the plane of the wave. V_{res} may be re-resolved into wave amplification V_{amp}, and wave rotation V_{rot}, components. In the case shown, V_{rot} produces rotation counter to the vortex direction and therefore corresponds to the short wavelength case of Fig. 6b,

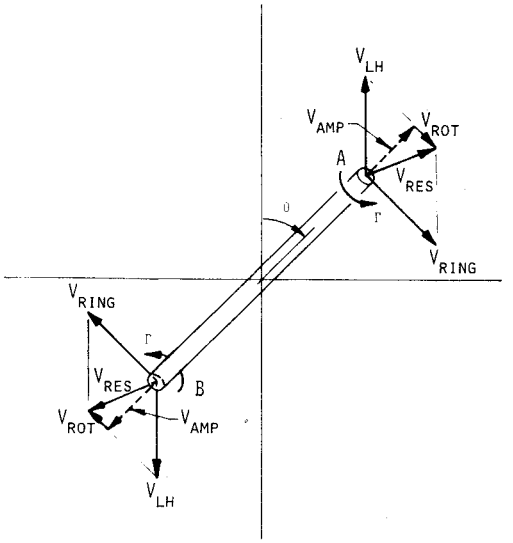

Fig. 7 Mechanism for opposing-sense vortex and wave rotation.

with looping inhibited. Decrease in V_{ring} (longer wavelength and/or larger core radius) or increase in V_{LH} (increased Γ and/or increased amplitude) would reverse V_{rot} and permit conventional looping.

IV. Multiple-Pair Convergence

A. Twin Pairs

Definition of Variables

In contrast to the previous cases, the spiral wavelength for a twin-pair trail is determined by aircraft forward speed, U_∞, as well as vortex details and it must be included in the normalization scheme. Define

$$\Gamma_F' = \frac{\Gamma_F}{U_\infty b/2} \qquad \Gamma_T' = \frac{\Gamma_T}{U_\infty b/2} \tag{6}$$

and

$$\phi = \Gamma_F' + \Gamma_T'$$

where b is tip span, Γ_F is flap vortex strength, and Γ_T is tip vortex strength.

For convenience, write

$$\gamma = \frac{\Gamma_T}{\Gamma_F} = \frac{\Gamma_T'}{\Gamma_F'} \tag{7}$$

The following relationships are noted

$$\Gamma_F' = \frac{\phi}{1+\gamma} \qquad \Gamma_T' = \frac{\gamma\phi}{1+\gamma} \tag{8}$$

$$\eta_F + \gamma\eta_T = (1+\gamma)\eta_{CG} \tag{9}$$

$$C_L/\mathcal{R} = \phi\eta_{CG}$$

where $\eta_T b$, $\eta_F b$, and $\eta_{CG} b$ are tip vortex, flap vortex, and vortex c.g. spans, respectively.

Time $t$sec) after aircraft passage is normalized via

$$\tau = \frac{tU_\infty}{b/2} \tag{10}$$

For multiple vortex arrays, the wavelength of spiral motions is defined in aircraft spans as λb. It may be shown that the

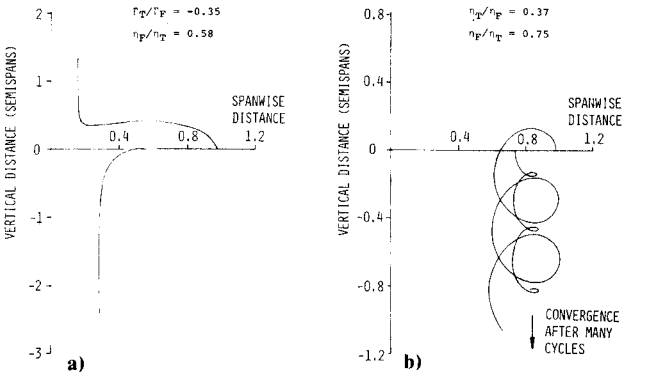

Fig. 8 Examples of a) transient and b) cyclic vortex motion; distances normalized on wing semispan.

time per revolution of Γ_F and Γ_T about their c.g., in two dimensions, is given by

$$\tau/\text{rev} = 4\pi^2 \frac{(1+\gamma)^2}{\phi} (\eta_T - \eta_{CG})^2 \tag{11}$$

provided that the center plane is not approached closely by a vortex trajectory. In aircraft variables

$$\tau/\text{rev} = 4\pi^2 \frac{\mathcal{R}}{C_L} \frac{(\eta_F + \gamma\eta_T)}{(1+\gamma)} (\eta_T - \eta_F)^2 \tag{12}$$

Also,

$$\lambda = 0.5\tau \text{ per rev.} \tag{13}$$

Parametric Classification of Twin Pairs

At low values of η_F/η_T and γ, two-dimensional studies[10] show that large vertical separation occurs between the two pairs, and the wake is dispersed. This may occur after a part-cycle or after many cycles of motion (see Fig. 8). A good approximation to the associated boundary in η_F/η_T and γ given in Ref. 10, is obtained by imposing the condition that the tip vortex intersects the center plane after 180 deg or less of travel. This yields

$$\eta_F \le \frac{1-\gamma}{2} \qquad \gamma \le 1 \tag{14}$$

Beyond this boundary, two-dimensional considerations show that the motion will persist indefinitely. However, if a finite wavelength, three-dimensional calculation is made, self-induction effects make finite lifetimes possible.

It is evident from Fig. 9 that, in cases beyond the region defined by Eq. (14), either the weaker or the stronger vortex may converge at the center plane. We note also that in each case either the flap or the tip vortex may be considered stronger if "conjugate" cases are considered (see Fig. 9 and Ref. 6) and appropriate rescaling is carried out.

Figure 10 is a parametric map with relative flap span as ordinate and relative vortex strength as abscissa. Each plotted point depicts one computer run similar to those shown in Fig. 9. Triangles and circles represent, respectively, flap and tip vortex convergence as the first event. As might be expected, tip vortex convergence occurs in the vicinity of the lower-left boundary (Eq. 14), but then flap vortex convergence becomes more likely as η_F is increased. With $\Gamma_T = \Gamma_F$, the chances of convergence are equal for flap and tip vortices and on crossing this line the identity of the convergent vortex switches as conjugate cases are encountered.

It is possible to predict the boundary between regions II and III (Fig. 10) by means of a simple analysis concerning the

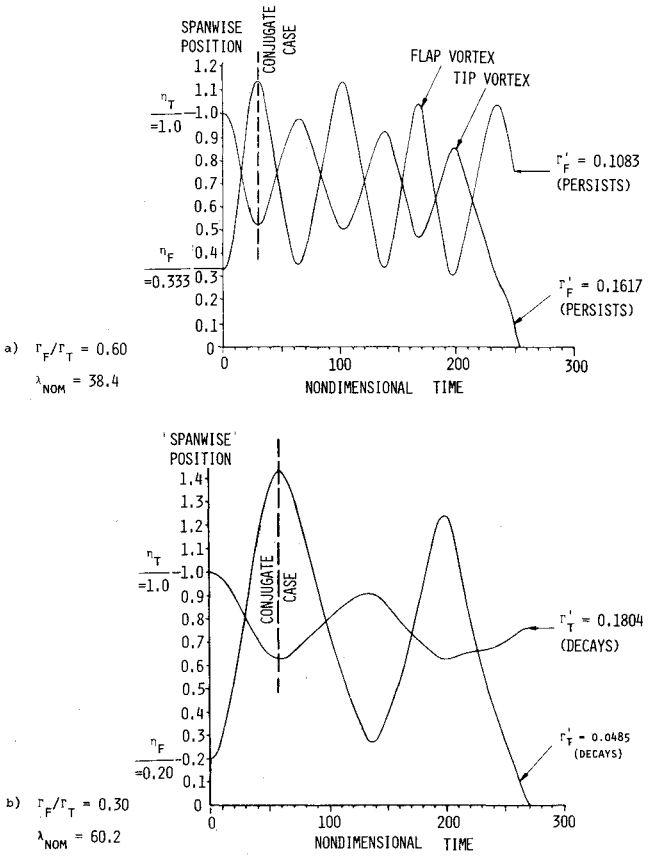

Fig. 9 Examples of flap- and tip-vortex convergence.

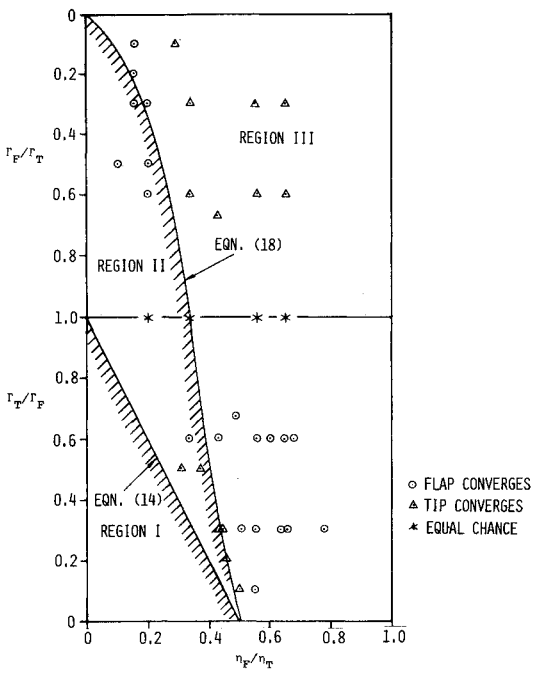

Fig. 10 Twin-pair parametric study: identification of the convergent vortex, $\lambda = 5.375$.

closest approach distance to the center plane of each vortex and the associated downwash increment. The closest approach distance $\eta_{\min}$ is given by

$$\eta_{\min} = \frac{2}{1+\gamma}(\eta_F + \gamma) - 1 \tag{15a}$$

for the tip vortex, and

$$\eta_{\min} = \eta_F \tag{15b}$$

for the flap vortex.

We define spiral strain indices σ_F and σ_T in terms of velocity occurring at the minimum positions. Thus

$$\sigma_F = \frac{\Gamma'_F}{\eta_{\min F}} \tag{16a}$$

and

$$\sigma_T = \frac{\Gamma'_T}{\eta_{\min T}} \tag{16b}$$

We now hypothesize that the vortex that has the larger σ value will converge first. Thus, for the tip vortex to converge first requires that

$$\sigma_T > \sigma_F$$

Using Eq. (15), this gives

$$\frac{\Gamma'_F \gamma(1+\gamma)}{2\eta_{F_{\text{crit}}} - (1-\gamma)} > \frac{\Gamma'_F}{\eta_{F_{\text{crit}}}} \tag{17}$$

for the tip vortex to converge first.

A borderline case may be found by using an equality in Eq. (17) which readily yields

$$\eta_{F_{\text{crit}}} = \frac{1}{\gamma+2} \tag{18}$$

This line partitions the data in Fig. 10 quite successfully, although not perfectly, because of the simplifying assumptions. Reference 6 shows that Eq. (17) identifies the flap and tip convergence regions correctly provided that appropriate care is taken in treating the inequality.

The Surviving Vortex

Figure 11a shows constant vortex strength contours for the flap and the tip vortices with total lift constant. The simple linear relationships evident in the lower half persist for $\Gamma_T/\Gamma_F > 1$ but are distorted in the upper part of the figure on encountering the Γ_F/Γ_T scale.

If Eq. (18) is overlayed on Fig. 11a and the surviving vortex strengths are picked out, Figure 11b results. It is immediately apparent that Regions I and II are undesirable because the stronger vortex survives. Thus, a strong inboard flap vortex certainly produces early tip vortex convergence at the center plane, but its own survival may prove hazardous unless some other mechanism hastens its destruction.

Time to Center-Plane Convergence

Figure 12a shows contours of time taken for vortices to converge at the center plane, in terms of the previous vortex strength and flap-span parameters. The greatest time shown, $\tau_c = 600$ corresponds to approximately five miles for a Boeing 747 in the approach condition with standard flaps. However, span-loading considerations show that the particular λ value chosen for Fig. 12a is too short for most jumbo-jets and further computations are required. Figure 12b, based on Eqs. (12) and (13), may be consulted to determine actual values of wavelength if the span-loading parameter, $C_L/\mathcal{R}$ is unknown.

B. Multiple Pairs

General Approach

For each vortex pair in a multicomponent system, there are at least three independent variables: vortex strength, span position, and core radius. Effective viscosity is a possible

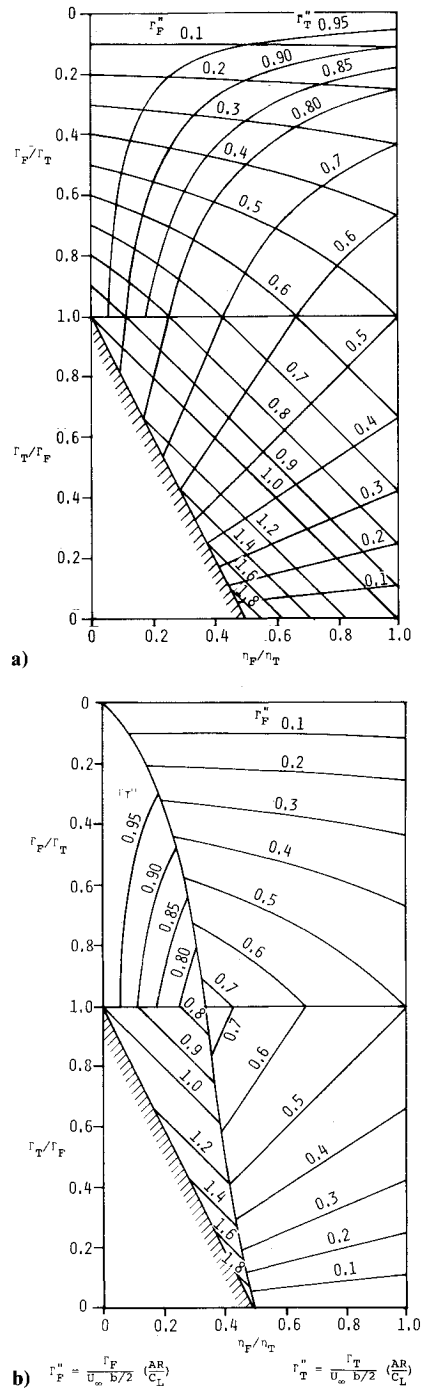

Fig. 11 Vortex strengths for twin-pair cases: a) relative vortex strengths for constant total lift; b) strength of the vortex remaining after convergence.

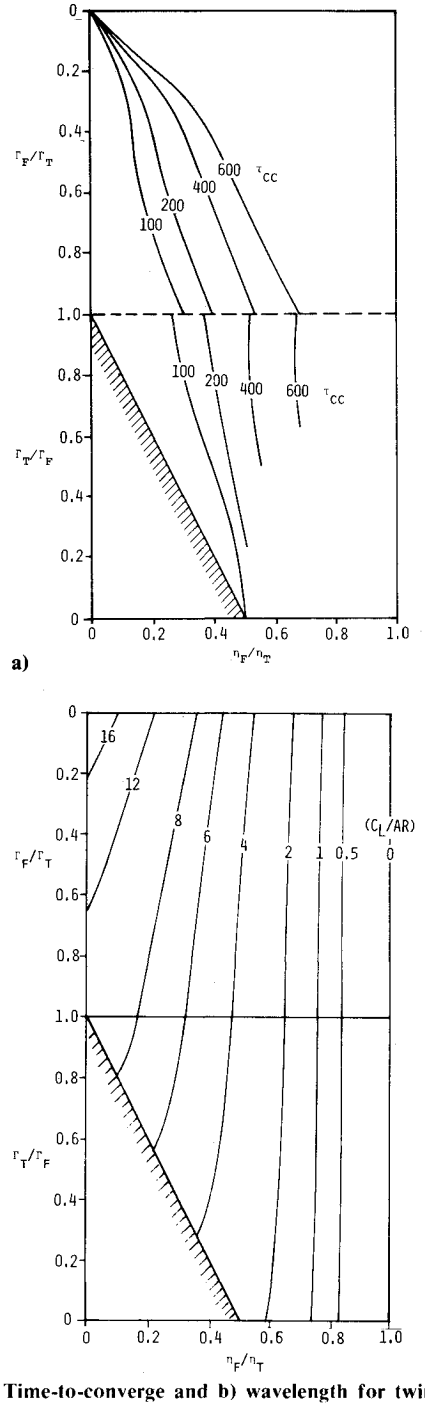

Fig. 12 a) Time-to-converge and b) wavelength for twin-pair case ($\lambda = 5.37$, $C_L/AR = 0.1714$).

fourth candidate. For N multiple vortices, there are thus $3N$ or $4N$ minus one variables. (Length scale may be embedded in the core Reynolds number.) These considerations, together with a strong impact upon computer mean time and storage requirements, make it highly desirable to eliminate from the calculation those vortices that converge early and to merge those that spiral together in close proximity. Figure 13 shows examples of both types. This particular case concerns a "sawtooth" loading configuration designed by Rossow[5] for early self-disruption. The reduction from seven to four vortex pairs is clearly most desirable, computationally.

The results shown in Fig. 13 were obtained using an aircraft-fixed two-dimensional calculation. Since complicated three-dimensional relaxation cases are likely to require individual treatment to overcome stability problems and are liable to be very expensive to run, it may be acceptable to rely on a simpler method for the early wake provided that the convergence or merging events are strongly indicated. If this is so, the predictive accuracy of the overall calculation will probably be acceptable.

The approach thus includes the following steps, given vortex dispositions along the trailing edge and their strengths:

1) Two-dimensional[11] or (preferably, if stable), three-dimensional relaxation methods are used to identify and treat each vortex merging and convergence to the center plane. This usually reduces the wake to three or four vortex pairs. The remaining wake is treated using aircraft-fixed methods until two pairs remain.

2) If the remaining twin pair is largely undistorted, and individual core details are not available, a parametric map is consulted.

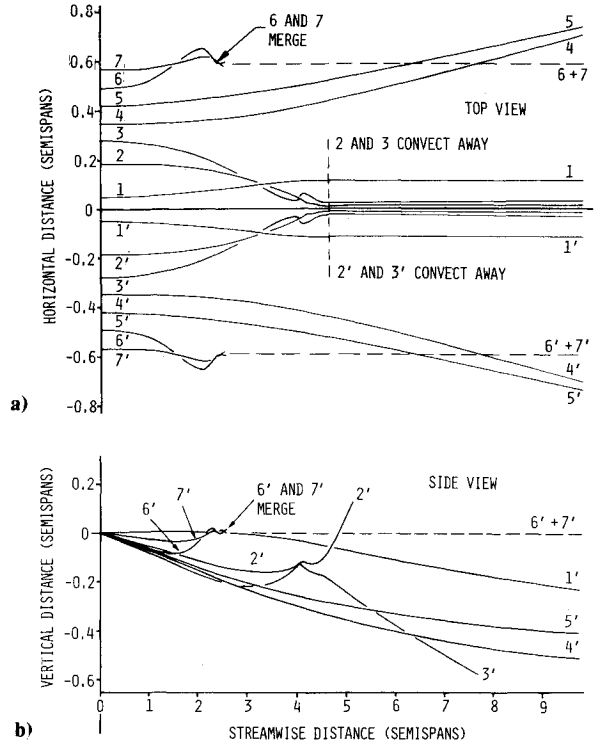

Fig. 13 Convergence and merging in the near-wake for multiple pairs for a) horizontal and b) vertical distances.

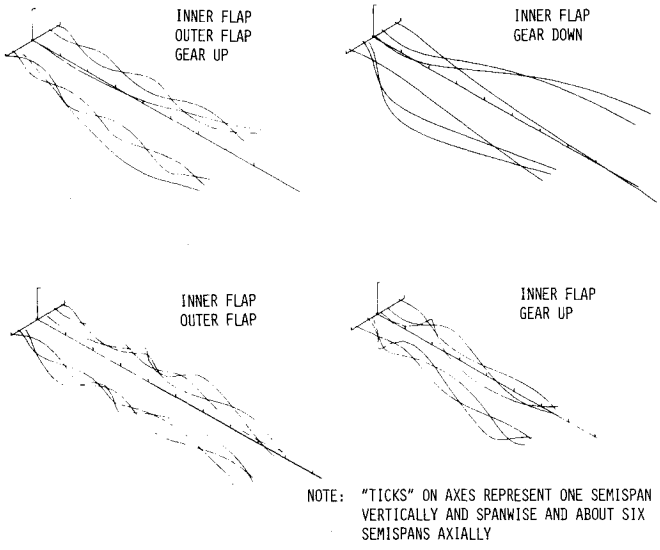

Fig. 14 Effect of the outboard flap and landing gear on the near-wake of a Boeing 747 on approach.

3) Once one member of the twin pair has either converged on the center plane or merged with its mate, the ensuing single pair wake must be treated via an appropriate viscous decay analysis for a straight vortex pair in still air. If it is possible to postulate a periodic disturbance, the methods of Sec. III may be used.

"Jumbo"-Jet Cases

Four Boeing 747 approach cases were selected in the light of recent wind-tunnel and flight wake hazard test experience at NASA concerning the effect of removing the outer flap and using the inner flap alone to restructure the vortex wake and concerning the effect of landing gear deployment on such results. In the present calculations, the representation of the gear is via its estimated effect upon span load: this omits all viscous wake considerations. Nonetheless, the gear-related span-load changes are found to have a significant impact upon the vortex wake structure. Preruns, to identify convergence, merging, etc., permitted simplifications to the distributions, such that three-pair configurations could be used. Three-dimensional relaxation of these three-pair configurations to a steady state then produced the wake structures shown in Fig. 14.

The upper two cases of Fig. 14 correspond to early flight tests that were carried out, gear-up, for full flaps and for inboard flaps only. Wider vortex dispersion is evident in the latter case, which should be beneficial. Lowering the gear reduced the strength of the (antilift) inboard flap vortex in both cases. With outer flaps present, lowering the gear caused a much less regular periodic near-wake solution. The reduction in inboard vortex strength, due to the gear, also greatly reduced the tendency of the flap and tip vortices to spread apart. A more hazardous wake is therefore implied with the gear down. This corresponds to flight test observations.

The results of Fig. 14 have not been extended to determine time-to-converge. Two-dimensional extensions of the B747 runs have been made indicating that convergence is occurring in the cases shown, but such runs can give no further information because curvature terms, which lead to convergence, are lacking.

V. Conclusions

Finite-element three-dimensional relaxation methods have been used to calculate the development of vortex wakes behind aircraft for a considerable downstream distance. The inclusion of a self-induction term in the solution, dependent upon local curvature and vortex core radius, permits calculation of finite lifetimes for systems for which infinite life would be predicted two-dimensionally. Single-pair, twin-pair, and multiple-pair studies are described. Although "jumbo" aircraft wake examples are included, these have not been carried out far enough for other than qualitative conclusions to be drawn.

The wake studies have led to the following conclusions and recommendations.

Single-Pair Wakes

1) There is a lower limit to the wavelengths at which the "Crow"-type instability can occur. Below this limit, self-induction effects cause the plane of the disturbance waves to rotate counter to the vortex direction.

2) Disturbance waves in a horizontal plane are several times more stable than the classic, 45-deg "Crow" case. Vertical and spiral waves are slightly more stable.

Multiple-Pair Wakes

3) There is an important distinction between single- and multiple-pair vortex convergence at the center plane. The first is usually a space-fixed event, but the latter moves at aircraft speed.

4) The self-induction term causes the time taken for vortices to converge at the center plane to be a strong function of wavelength. Either vortex can converge first.

5) As a result of the above, there appears to be maximum, in time-to-converge, when flap span lies between 40 and 60% of wing span. Expanded studies are needed to define the effects of span loading on such results.

6) Pilot studies of Boeing 747 configurations show correct qualitative response to removal of the outer flap and to gear deployment, as compared with wind-tunnel and flight-test experience.

7) More detailed studies should be undertaken of the separate effects of vortex core radius and relaxed wavelength on the time to attain center-plane convergence in twin-pair cases. This should provide useful design guidance for low-hazard wakes.

8) Further time-to-converge twin-pair parametric studies (see Sec. IV) should be carried out, holding $C_L/\mathcal{R}$ constant for each of several maps like Fig. 12a.

Acknowledgments

The present work was carried out under NASA Contract NAS2-8651 under the guidance of V. J. Rossow. The authors greatly appreciate both Rossow's helpful comments and the computing help tendered by Opal J. Lemer in performing runs on the CDC 7600 computer.

References

[1] Crow, S. C., "Stability Theory for a Pair of Trailing Vortices," *AIAA Journal*, Vol. 8, Dec. 1970, pp. 2172-2179.

[2] Hackett, J. E. and Theisen, J. G., "Vortex Wake Development and Aircraft Dynamics," *Aircraft Wake Turbulence and Its Detection*, edited by J. Olsen, A. Goldberg, and M. Rogers, Plenum Press, New York, 1971.

[3] Chevalier, H., "Flight Test Studies of the Formation and Dissipation of Trailing Vortices," *Journal of Aircraft*, Vol. 10, Jan. 1973, pp. 14-18.

[4] Widnall, S. E., Bliss, D. B., and Zalay, A., "Theoretical and Experimental Study of the Stability of a Vortex Pair," *Aircraft Wake Turbulence and Its Detection*, edited by J. Olsen, A. Goldberg, and M. Rogers, Plenum Press, New York, 1971.

[5] Rossow, V. J., "Theoretical Study of Lift-Generated Vortex Wakes Designed to Avoid Roll-Up," *AIAA Journal*, Vol. 13, April 1975, pp. 476-484.

[6] Evans, P. F. and Hackett, J. E., "Numerical Studies of Three-Dimensional Breakdown in Trailing Vortex Wakes," NASA CR-137888, June 1976.

[7] Rossow, V. J., "Convective Merging of Vortex Cores in Lift-Generated Wakes," AIAA Paper 76-415, AIAA 9th Fluid and Plasma Dynamics Conference, San Diego, Calif., 1976.

[8] Leonard, A., "Numerical Simulation of Interacting, Three-Dimensional Vortex Filaments," *Proceedings of the 4th International Conference on Numerical Methods in Fluid Dynamics*, Springer-Verlag, Heidelberg, 1974.

[9] Lamb, Sir Horace, *Hydrodynamics*, 6th ed., Dover, New York, 1945, p. 211.

[10] Bilanin, A. J., Donaldson, C. duP., and Snedeker, R. S., "An Analytical and Experimental Investigation of the Wakes Behind Flapped and Unflapped Wings," AFFDL-TR-74-90, May 1974.

[11] Hackett, J. E. and Evans, M. R., "Vortex Wakes Behind High-Lift Wings," *Journal of Aircraft*, Vol. 8, May 1971, pp. 334-340.